



Review

A multi-agent cell-based model for wound contraction

W.M. Boon ^a, D.C. Koppenol ^b, F.J. Vermolen ^{b,*}^a Department of Mathematics, Universitetet i Bergen Realfagbygget, Allégt. 41, 5020 Bergen, Norway^b Delft Institute of Applied Mathematics, Faculty of Civil Engineering, Delft University of Technology, Mekelweg 4, 2628 CD Delft, The Netherlands

ARTICLE INFO

Article history:

Accepted 22 November 2015

Keywords:

Cell-based modelling
 Finite-element method
 Immune system response
 Hybrid approach
 Wound contraction

ABSTRACT

A mathematical model for wound contraction is presented. The model is based on a cell-based formalism where fibroblasts, myofibroblasts and the immune reaction are taken into account. The model is used to simulate contraction of a wound using point forces on the cell boundary and it also determines the orientation of collagen after restoration of the damage. The paper presents the mathematical model in terms of the equations and assumptions, as well as some implications of the modelling. The present model predicts that the amount of final contraction is larger if the migration velocity of the leukocytes is larger and hence it is important that the immune system functions well to prevent contractures. Further, the present model is the first cell-based model that combines the immune system to final contractions.

© 2015 Elsevier Ltd. All rights reserved.

Contents

| | |
|--|------|
| 1. Introduction | 1388 |
| 2. The mathematical model | 1390 |
| 2.1. The biological entities | 1390 |
| 2.2. The mathematical formalism | 1390 |
| 2.2.1. Decay of fibrin and collagen regeneration | 1390 |
| 2.2.2. Secretion and decay of the cytokines | 1391 |
| 2.2.3. Cell dynamics | 1391 |
| 2.2.4. Collagen synthesis and contact guidance | 1393 |
| 2.2.5. The mechanical model | 1393 |
| 3. Numerical solution method | 1394 |
| 3.1. The chemical entities | 1394 |
| 3.2. The mechanical balance | 1396 |
| 3.3. The cell migration | 1396 |
| 4. Numerical simulation results | 1397 |
| 4.1. The basis run | 1397 |
| 4.2. Parameter variation | 1398 |
| 5. Discussion and conclusions | 1400 |
| Conflict of interest | 1401 |
| Acknowledgements | 1401 |
| Appendix A. Supplementary data | 1401 |
| References | 1401 |

1. Introduction

An important subprocess during wound healing is wound contraction. During this process, the damaged tissue gets pulled together in order to close the wound rapidly and minimise the

* Corresponding author.

E-mail addresses: Wietse.Boon@uib.no (W.M. Boon),
D.C.Koppenol@tudelft.nl (D.C. Koppenol), F.J.Vermolen@tudelft.nl (F.J. Vermolen).
 URL: <http://twi.ta.tudelft.nl/users/vermolen> (F.J. Vermolen).

chance of infection. Naturally, this is a desirable effect for wounds, but when the contraction is too large, it can become a negative side-effect. In that case, a permanent contraction known as a contracture can be the result. This may lead to problems such as functional restrictions (Enoch and Leaper, 2008). A major difference between scar tissue and undamaged tissue lies in the alignment of its fibers (Cumming et al., 2010). While undamaged tissue has an isotropic pattern of interwoven collagen bundles, scar tissue is characterised by fibers aligned in only a few directions. This anisotropy causes the tissue to have inferior strength and flexibility. Clark et al. (2014) and Murphy et al. (2012) state that the regenerated tissue has only 70% of the normal dermal strength. Furthermore, the reduction in flexibility can cause major problems for the affected patient (Hinz, 2006).

Because of the great implications that contraction has on the final stages of skin repair, it serves as an interesting component in a wound healing model. By combining the mechanical implications due to contraction with some of the biological processes of dermal wound healing, we aim at creating a more complete view of the entire wound healing process. Such a model may lead to a better understanding of the wound healing process which is essential for the development of new procedures to reduce contracture formation in the resulting scar tissue. Fibroblasts and myofibroblasts are the primary factors involved in the process of contraction. In this process, the cells adhere to the extracellular matrix (or ECM). The ECM is comprised mostly of collagen fibrils (Enoch and Leaper, 2008). They then pull together these collagen fibrils and consequently compact the connective tissue (Clark et al., 2014). The difference between the cells is that myofibroblasts will exert stronger contractile forces than fibroblasts (Hinz, 2006). An abundance of contraction may result in the permanent contraction (i.e. the contracture) of the wound which remains after all fibroblasts and myofibroblasts have either died or left the wound area. Furthermore, both fibroblasts and myofibroblasts will initiate the synthesis of the oriented collagen fibrils in the wound. These form the building blocks for the new ECM which replaces the fibrin clot. These collagen fibrils themselves act as a guidance cue for subsequently arriving fibroblasts. Hence, there is a constant interaction where fibroblasts affect the orientation of the collagen matrix and the orientation of this collagen matrix influences the movement of fibroblasts (McDougall et al., 2006).

Since there is an extensive amount of literature available on the mathematical modelling of dermal wound healing, we will limit our review to the most relevant articles for the present work. Hence we focus on articles concerning the mathematical modelling of the contraction process and the orientation of the collagen bundles in the dermis during dermal wound healing. In the field of wound contraction modelling, Tranquillo and Murray (1992) were one of the first to propose a mathematical model for wound healing that takes the contraction process into account. The model presented in this work offered a general framework for understanding how traction exerted by wound fibroblast eventually results in wound contraction. The equations described here formed the basis for much of the computational research in this field. From this model, the model by Olsen et al. (1995, 1996) is based on a deterministic formalism to investigate key clinical problems in wound healing disorders. The focus was on contraction and simplifications were made such that only the essential roles of fibroblasts and myofibroblasts were described along with a single chemical growth factor and the ECM. The results showed that a distinction needed to be made between contraction during the proliferation stage and the prolonged remodeling of collagen during the remodeling stage. Later models for wound contraction were developed by Javierre et al. (2009) and Valero et al. (2014, 2015), where in the latter study, non-isotropies were dealt with via a neo-Hookean formulation for the strain energy density. The

last-mentioned work does not consider contact guidance of the cells according to the fibre orientation, but it is very useful in linking fiber orientation to mechanical properties.

Another significant contribution to this field was the model by Murphy et al. (2012). This model incorporated the interaction between fibroblasts and the ECM combined with a more realistic modelling of cytokines. Contraction was investigated in a one-dimensional model activated by TGF- β . Here, the cytokine and mechanical tension were assumed to be responsible for the differentiation from fibroblast to myofibroblast. The model then showed that the removal of TGF- β and reduction of tension resulted in a decrease in the number of myofibroblasts and therewith a reduction in contraction. A major shortcoming of these early works, however, is that a contracture is not a stable solution within these models. With respect to the dynamics of fiber bundle orientation, one of the most important mathematical theories was formulated by Barocas and Tranquillo (1997). In this work, an anisotropic biphasic theory for tissue-equivalent mechanics was presented. This theory can account for fibril alignment during wound healing and introduced cell contact guidance. Although the theory was formulated in a general sense, it was speculated that it may be valid for physiological processes such as wound contraction (Barocas and Tranquillo, 1997). Later, the dynamics of fiber bundle orientation was incorporated into a dermal wound healing model by Olsen et al. (1999). Here, two approaches were proposed for modelling the cell populations. First, the cell densities were modeled as continua. This continuum approach resulted in a system of partial differential equation on a macroscopic scale. However, patterns of alignment on microscopic length scales were lost in this approach. Therefore, a novel approach was introduced in which cells are presented as discrete individuals and the ECM as a continuum. This hybrid model produced the desired results on both scales.

The modeling of the interaction between cells and the ECM alignment was developed further by Dallon et al. (2000, 1999, 2001) by including ECM production and decay. In all cases, the cells were considered as discrete objects while the matrix was modeled as a continuum. In Dallon et al. (1999), various aspects of the cell interactions with collagen and fibrin were investigated first in order to find which alignment properties arise in different cases. These aspects included cell speed, flux, polarisation, density, initial matrix orientation and the influence of cells on the matrix. The results showed that all of these factors had a certain effect on the alignment of collagen. It was shown next by Dallon et al. (2000) that of these factors, cell speed and the positions where fibroblasts enter the wound area are the most influential on fiber alignment. Within the model, the matrix orientation was modeled using a vector field. This implied that the orientation of the bundles was unidirectional. In a third article, Dallon et al. (2001) incorporated a time-variant concentration field for the cytokine TGF- β to the model and the effects of different profiles of this cytokine were investigated. It was found that the influence TGF- β has on changes in cell motility, proliferation and collagen production had little effect on collagen matrix alignment. Furthermore, it was shown that the alignment of the new tissue depends highly on the fibroblast reorientation rate.

A couple of years later, a further investigation was conducted by McDougall et al. (2006) on the effects of different cytokine concentrations. They made an important distinction between the degree of scarring and wound integrity. It was shown that a large chemoattractant diffusion coefficient results in an optimised wound integrity while the degree of scarring is decreased when a competitive inhibitor to TGF- β is introduced. From the vector-based representations of collagen bundles and fibrin fibers used by Dallon et al. (1999) and McDougall et al. (2006), a few drawbacks can easily be deduced. First, there is no measure available for the

degree of isotropy of the field at a point. Second, a vector-based approach is unidirectional while fiber bundle alignment works in a bidirectional manner. In order to overcome both these limitations, Cumming et al. (2010) have presented a tensorial approach to collagen bundle orientation based on the earlier work of Barocas and Tranquillo (1997). The model presented by Cumming et al. (2010) further incorporates several of the main biological subprocesses which make up the dermal wound healing process. The model was particularly extensive since a total of six species were incorporated ranging from discrete cells to the continuum tensorial approach of the ECM. This model will serve as a basis for this study, where we incorporate the mechanical pulling of (myo-) fibroblasts on the extracellular matrix. The pulling forces are computed via the principles of a series of point sources on the cell boundary as outlined in Vermolen and Gefen (2015). This approach has some similarities with the immerse boundary method for computation of surface forces over bodies that move within a fluidic medium.

The paper is organised as follows: we start with a presentation of the model in terms of the biological assumptions and mathematical relations, subsequently the methods that are used are presented, which is followed by the presentation of the simulation results and finally we present some conclusions.

2. The mathematical model

The (mechano-)biology behind wound healing and contraction is extremely complicated. There is a huge chain of chemokines (growth factors) that are secreted and received by cells of the various phenotypes involved. The review by Barrientos et al. (2008) provides a list of growth factors and chain of interactions between them in terms of secretion and their role on the behaviour of the cells involved. In Barrientos et al. (2008), the reader is referred to experimental and clinical studies on how the growth factors influence the behaviour of cells in terms of migration, proliferation or production of extracellular matrix in the case of fibroblasts. In Barrientos et al. (2008), it is reported that TGF- β recruits fibroblasts as well as inflammatory cells to the wound site. In Postlethwaite et al. (1987, 1978), it was experimentally found that human fibroblasts migrate towards the gradient of TGF- β . This conclusion was also drawn in Dallon et al. (2001) on the basis of the experimental study in Ellis and Schor (1996). In Pierce et al. (1991) and Deuel et al. (1982), it was experimentally concluded that leukocytes migrate towards gradients of PDGF, whereas in Seppä et al. (1982), it was found that fibroblasts also migrate in the direction of PDGF. In Cesarman-Maus and Hajjar (2005), the mechanism of fibrinolysis (decay of fibrin matrix) as a result of exposure to tPA was investigated experimentally. Combining all these experimental studies, some of the experimental studies seem to contradict each other. To keep the treatment accessible, in the modelling, several simplifications have been implemented, where we only incorporate attraction of the immune cells towards the gradient of platelet derived growth factor, and where the fibroblasts are attracted by the gradient of TGF- β . This treatment allows the simulation of the chain of biological processes such as the immune cells and the ingress of fibroblasts as consecutive, partly overlapping phases.

In the modelling, a two-dimensional surface section is considered. The domain contains an initially wounded or damaged portion and an initially undamaged section. The domain of computation is simplified by a rectangular domain where we assume that the boundaries are sufficiently far away from the wound region so that their influence is negligible. We present the various components of the model. First we start with listing the biological

entities that are involved in the model. Subsequently, the equations behind the model are presented and motivated.

2.1. The biological entities

The entities that we consider are divided into three categories: cells, cytokines and fibres. The cells are taken into account as discrete individual objects that move continuously through the dermis. To keep the model tractable, only fibroblasts, myofibroblasts and leukocytes are considered as phenotypes in the current modelling. The leukocytes are responsible for the clearing of the debris and for producing cytokines that attract fibroblasts and make them differentiate to myofibroblasts. In the current modelling, the cleaning function by the leukocytes is not incorporated. The interested reader is referred to **Vermolen et al. (2015) for the incorporation of the engulfment mechanism by the leukocytes on pathogens. Both fibroblasts and myofibroblasts secrete and reorient collagen bundles and exert forces on their surrounding environment, thereby causing contraction. We will assume that the myofibroblasts cause contraction at later stages of the wound healing process. The behaviour of the fibroblasts and myofibroblasts only differs in the phase of contraction. Therefore, we label whether each cell is fibroblast or myofibroblast during the simulation. For each cell, we take into account a certain number of receptors that are bound to a certain cytokine and this number of receptors has a direct influence on the behaviour of the cell.

The cytokines are responsible for fibrin decay and for the attraction of various cell species towards the wound region. Their concentrations are modelled as continuous variables over time and over the domain of computation as solutions to reaction-transport partial differential equations. In this study, we consider the following three species: tPA for fibrin decay, PDGF for leukocyte attraction (secreted earlier by the platelets), and TGF- β for the attraction of (myo)fibroblasts.

Finally, two collagen fibres are considered in the present modelling: collagen and fibrin. The fibrin density plays a role in the inflammatory phase only. Further, the density of collagen bundles plays an important role throughout the entire wound healing process. These densities influence the diffusion of cytokines, cell migration and the magnitude of the contractile forces. It is also noted that the (myo)fibroblasts migrate according to the orientation of the collagen bundles towards the wound area.

2.2. The mathematical formalism

In this section, the mathematical problem is posed in terms of equations and boundary/initial conditions. The initial domain of computation is given by a rectangle denoted by Ω , where the boundary consists of Γ_1 and Γ_2 , where Γ_1 represents a boundary of symmetry. The initial wound area is adjacent to the line of symmetry. All cells are treated as individual cells with a circular projection, and the chemical entities are treated using reaction-transport equations. Further mechanical equilibrium and Hooke's Law are assumed to describe the displacements and stresses over the domain of computation. First the collagen is described, subsequently the dynamics of the chemical entities are presented and finally, the migration of cells is given in terms of stochastic differential equations.

2.2.1. Decay of fibrin and collagen regeneration

It is assumed that the initial wound consists of completely formed fibrin network. This fibrin decays as a result of the chemokine tPA, whose concentration is denoted by $c_t = c_t(t, \mathbf{x})$ on time t and on position \mathbf{x} within the domain of computation. The domain of computation is characterised by the volume fractions of fibrin and collagen, respectively, denoted by $\rho_f = \rho_f(t, \mathbf{x})$ and

$\rho_c = \rho_c(t, \mathbf{x})$. The decay of collagen is modelled by

$$\frac{\partial \rho_f}{\partial t} = -r_p c_t \rho_f, \quad (1)$$

supplemented with a regularised initial condition stating unity in the initially wounded region and a zero value in the undamaged region. Note that $\rho_f + \rho_c = 1$ in Ω and for $t=0$, where Ω denotes the domain of computation and hence we only take ρ_f , the density of the fibrin, into account.

2.2.2. Secretion and decay of the cytokines

The dynamics of the various cytokines are described sequentially.

Tissue Plasminogen Activator (tPA): The first entity we describe is the concentration of tissue Plasminogen Activator (tPA), which is released by the endothelial cells that are the main building block of the small blood vessels. This cytokine breaks down the clot and hence it decays the fibrin. The production and diffusion is modelled by

$$\frac{\partial c_t}{\partial t} - \nabla \cdot (D^t(\rho_f) \nabla c_t) = T_t, \quad (2)$$

where T_t denotes the source as a result of the small blood vessels on the edge of the wound. Since it is known that diffusion in the fibrin is slower than in the collagen network, it is assumed that the diffusivity of tPA is given by

$$D^t = D^t(\rho_f) = \rho_f D_f^t + (1 - \rho_f) D_c^t, \quad (3)$$

where D_c and $D_f < D_c$, respectively, denote the tPA diffusivities outside of fibrin and in fibrin. The reaction term T_t is high over the edge of the wound, and zero in the rest of the domain. Let Γ_w be the wound boundary, that is the interface between the initially damaged and undamaged portion of the domain, then we use

$$T_t(t, \mathbf{x}) = s_t \delta_{\Gamma_w}(\mathbf{x}), \quad (4)$$

where s_t is the secretion rate, and δ_Γ represents a modified Dirac Delta distribution defined as follows:

- Let Γ be a curve in Ω , and $\delta_\Gamma : \Omega \rightarrow \mathbb{R}$ then

$$\delta_\Gamma(\mathbf{x}) : \begin{cases} = 0, & \mathbf{x} \notin \Gamma, \\ > 0, & \mathbf{x} \in \Gamma. \end{cases} \quad (5)$$

- Further, let $Q \subset \Omega$ and let $\mu : \Gamma \rightarrow \mathbb{R}^+$ represent the length of any curve Γ , then

$$\int_Q \delta_\Gamma(\mathbf{x}) d\Omega = \frac{\mu(Q \cap \Gamma)}{\mu(\Gamma)}. \quad (6)$$

Initially, it is assumed that there is no tPA, that is $c_t(0, \mathbf{x}) = 0$ in Ω . The boundary conditions either represent symmetry or a homogeneous Robin condition saying that far away the tPA content vanishes, that is

$$D^t(\rho_f) \frac{\partial c_t}{\partial n} + \kappa c_t = 0, \quad t > 0, \quad \mathbf{x} \in \Gamma_2. \quad (7)$$

Platelet Derived Growth Factor (PDGF): The next phase in the healing process is featured by the arrival of leukocytes. These cells are attracted towards the wound site by high concentrations of various chemo-attractants. In Cumming et al. (2010), these concentrations are simplified into one chemical species, however, since these leukocytes also secrete cytokines themselves through which they are attracted, they tend to cluster in areas with high concentrations of chemokines that they produced themselves. Since this behaviour is unrealistic, we distinguish between the cytokines secreted by the leukocytes and its chemoattractant. We

choose the attractant PDGF to account for this. The field of the PDGF attractant is modelled by a diffusion equation where initially its concentration is high in the initial wound region as a result of its production by the platelets. Let $c_p = c_p(t, \mathbf{x})$ denote the PDGF content, then we have

$$\begin{aligned} \frac{\partial c_p}{\partial t} - D_p \Delta c_p &= 0, \quad t > 0, \quad \mathbf{x} \in \Omega, \\ D \frac{\partial c_p}{\partial n} &= 0, \quad t > 0, \quad \mathbf{x} \in \Gamma_1, \\ D \frac{\partial c_p}{\partial n} + \kappa_p c_p &= 0, \quad t > 0, \quad \mathbf{x} \in \Gamma_2, \\ c_p(0, \mathbf{x}) &= \frac{1}{8} (1 + \tanh(5(2+x)))(1 + \tanh(5y)), \quad \mathbf{x} \in \Omega. \end{aligned} \quad (8)$$

This chemoattractant triggers the leukocytes to migrate towards the wound site and also triggers the leukocytes to leave the small blood vessels in the vicinity of the wound edge. This will be explained later, where cellular migration and contact forces are presented.

Transforming Growth Factor β (TGF- β): As mentioned earlier, we also have to consider the chemical TGF- β , which is secreted by the leukocytes and attracts the fibroblast to migrate into the wound. To this extent, using the same boundary conditions, we solve the following partial differential equation:

$$\begin{aligned} \frac{\partial c_\beta}{\partial t} - \nabla \cdot (D^\beta \nabla c_\beta) &= T_\beta(t, \mathbf{x}), \quad t > 0, \quad \mathbf{x} \in \Omega, \\ D \frac{\partial c_\beta}{\partial n} &= 0, \quad t > 0, \quad \mathbf{x} \in \Gamma_1, \\ D \frac{\partial c_\beta}{\partial n} + \kappa_\beta c_\beta &= 0, \quad t > 0, \quad \mathbf{x} \in \Gamma_2, \\ c_\beta(0, \mathbf{x}) &= 0, \quad \mathbf{x} \in \Omega. \end{aligned} \quad (9)$$

The sourcing term T_β represents the secretion by the leukocytes, in the presence of collagen and fibrin networks. Further, the diffusivity of TGF- β is described by

$$D^\beta = D^\beta(\rho_f) = \rho_f D_f^\beta + (1 - \rho_f) D_c^\beta, \quad (10)$$

Let $\mathbf{x}_i^l(t)$ denote the spatial position of the leukocyte with index i at time t , where $i \in \{1, \dots, N_l(t)\}$, and where $N_l(t)$ denotes the number of leukocytes at time t , then we have

$$T_\beta(t, \mathbf{x}) = c_{max} \sum_{i=1}^{N_l(t)} \left[(1 - \rho_f(t, \mathbf{x}_i^l(t))) c_{fib} + \rho_f(t, \mathbf{x}_i^l(t)) \right] \delta(\mathbf{x} - \mathbf{x}_i^l(t)), \quad (11)$$

where $\delta(\cdot)$ denotes the Dirac Delta distribution, further c_{max} and c_{fib} , respectively, denote a sourcing strength and a weighing factor.

2.2.3. Cell dynamics

As mentioned earlier, the cells are represented by circular projections on the extracellular matrix, and their positions at time t are denoted by $\mathbf{x}_i^l(t)$ and $\mathbf{x}_i^f(t)$ for the leukocytes and fibroblasts, respectively. The migration of both cell types is determined by the binding of the receptors on the cell boundary. Let $n^i(t)$ be the portion of bound receptors of cell i , then if i is a leukocyte, then

$$\frac{\partial n^i}{\partial t} = -\beta_p n^i + \gamma_p c_p(1 - n^i), \quad \beta_p, \gamma_p > 0, \quad n(0) = 0. \quad (12)$$

Here β_p and γ_p , respectively, account for the natural unbinding of receptors, and the factor for receptor binding to PGDF, all corresponding to cell i , if cell i is a leukocyte. Note that the PDGF concentration c_p determines the binding rate. If cell i is a fibroblast, then the kinetics of the receptor binding is determined by the concentration of TGF- β and given by

$$\frac{\partial n^i}{\partial t} = -\beta_\beta n^i + \gamma_\beta c_\beta(1 - n^i), \quad \beta_\beta, \gamma_\beta > 0, \quad n(0) = 0. \quad (13)$$

It is reassured that the portion never exceeds unity. As the overall concentration of cytokines, being either TGF- β and PDGF, respectively, decays over time, the cell receptors will unbind over time. This implies that the fibroblasts and leukocytes will lose activity as time proceeds. The increase of the number of receptors first influences the movement of the leukocytes. As presented in Cumming et al. (2010), the cells are modeled as discrete disks moving over the domain of computation. We adjust the equation due to Cumming et al. (2010) using the following insights from Enoch and Leaper (2008): The extracellular matrix, composed of collagen mostly, is a critical cell movement regulator. Further, we take into account that the tissue in the upper part of the dermis (the papillary dermis) contains loosely collagen fibers (Marks and Miller, 2013). Therefore, we assume that the cell migration speed decreases as they move deeper away into the wound area. The reason for this is that the cells less easily find rigid spots to adhere to in the loosely connected regions. Herewith, we use the following relation for the magnitude of the leukocyte velocity:

$$v_i^l = v_{max}^l(1 - k\rho_f) \left(1 - \exp\left(-\text{dist}\left(\mathbf{x}_i^l(t), \Gamma_N\right)\right)\right) \left(\frac{1}{4} + \frac{4}{3 + 80(1 - n^i)^6}\right), \quad (14)$$

where Γ_N represents the line of symmetry of the wound, and $\text{dist}(\mathbf{x}, \Gamma)$ represents the minimal distance between position \mathbf{x} and the curve Γ . This factor takes into account that the cell migration velocity decreases as the cells move deeper into the wound area. For the actual movement of the leukocytes, we take into account chemotaxis, as well as random walk. To this extent, for the case that there is no mechanical intercellular contact, the migration speed of the leukocytes is given by

$$d\mathbf{x}_i^l(t) = v_i^l \gamma_l(1 - n^i) \frac{\nabla c_P(\mathbf{x}_i^l(t))}{1 + \|\nabla c_P(\mathbf{x}_i^l(t))\|} dt + \sqrt{2D_l} d\mathbf{W}(t), \quad (15)$$

where $\mathbf{W}(t)$ denotes the vector-Wiener process and D_l denotes the diffusivity of the leukocytes. First, we discuss the dynamics of the leukocytes. Around the wound section, the tissue is undamaged and containing small blood vessels from which leukocytes arrive into the extravascular tissue around the blood vessels. The actual number of blood vessels that arrive into the domain depends on the concentration of PDGF. To this extent, we use a Poisson process to account for the number of leukocytes that arrive per unit of time. We assume that $N(t)$, which is the counting process for the number of leukocytes appearing on the wound edge, denoted by $W(t)$, obeys a Poisson process, which is characterised by

- $N(0) = 0$.
- The process has independent increments.
- The number of events in any interval of length t is Poisson distributed with mean λt , that is for all $s, t > 0, m \in \mathbb{N}$:

$$\mathcal{P}(N(s+t) - N(s) = m) = \exp(-\lambda t) \frac{(\lambda t)^m}{m!},$$

where $\mathcal{P} : \mathbb{N} \rightarrow [0, 1]$ denotes the probability.

The expected value for the number of leukocyte counts over a time interval of length Δt is given by $\mathcal{E}(N_{\Delta t}) = \lambda \Delta t$. Let $L(W(t))$ denote the length of the wound edge, then we assume that $\lambda = \beta c_P L(W(t))$ which accounts for an increase of the number of entering leukocytes with increasing PDGF content. Having the number of leukocyte counts, we position the entering leukocytes on the rim of the wound Γ_w . Once the number of leukocytes that appear on wound edge $W(t)$, we use a uniform distribution for the position of each leukocyte on $W(t)$, where we parametrise the wound edge by

the curve distance over $W(t)$ from the upper-left corner point, denoted by L , herewith we use the following probability density function for leukocyte j :

$$L_j \sim U[0, L(W(t))]. \quad (16)$$

Next, we treat the fibroblasts. The equation of migration of fibroblasts is analogous to the relation of migration of leukocytes with the subtle difference that the fibroblasts move according to the gradient of TGF- β . Then the relation is given by

$$d\mathbf{x}_i^f(t) = v_i^f \gamma_f(1 - n^i) \frac{\nabla c_\beta(\mathbf{x}_i^f(t))}{1 + \|\nabla c_\beta(\mathbf{x}_i^f(t))\|} dt + \sqrt{2D_f} d\mathbf{W}(t), \quad (17)$$

The above equation does not yet contain collagen guidance as a result of the orientation of the fibers, as well as it does not yet contain the contribution as a result of contact forces that cells exert on each other. An important difference between the (myo) fibroblasts and leukocytes is that (myo)fibroblasts proliferate once a minimum proportion of receptors, \tilde{n} , is chemically bound for a certain amount of time. To this extent, a timer τ_i^f is introduced for each fibroblast i , that follows:

$$\tau_i^f(t + \Delta t) = \tau_i^f(t) + \begin{cases} \Delta t, & n^i > \tilde{n}, \\ 0, & n_i \leq \tilde{n}. \end{cases} \quad (18)$$

A second threshold is obtained by computing the number of cells in the nearby region to approximate the cell density, then it is determined whether the cells have a sufficient amount of space to divide.

Next to the chemotactic and random walk modes for cell migration, we consider cell migration as a result of contact forces that cells exert to each other. This mode of migration is treated in the same way as in Vermolen and Gefen (2012). In this method, the distance between the cell centres is computed, if this distance is less than the sum of both cell radii, then the cells are displaced over the line that connects the colliding cells. The details can be found in Vermolen and Gefen (2012).

Cell death is treated as a stochastic process, where it is assumed that the probability of cell death is *memoryless*, which means that the event of death within the time-interval Δt does not depend on the cell evolution over the period before t . In this study, we use an exponential probability distribution with probability density, under assumption that the cell was alive on time t , given by

$$f_D(s | t) = \frac{1}{t_D} e^{-(t+s)/t_D}, \quad (19)$$

where t_D is the expected time of death at each time t . This probability density implies that the probability of cell death over the interval Δt is given by

$$\mathcal{P}_D(t + \Delta t | t) = \int_t^{t + \Delta t} f_D(s | t) ds = 1 - e^{-\Delta t/t_D}, \quad (20)$$

where $\mathcal{P}_D(t + \Delta t | t)$ denotes the probability that the cell dies within the interval $(t, t + \Delta t)$ (given that the cell was alive at time t from a probabilistic point of view). It is assumed that the expected life span of the leukocytes cells is determined by the PDGF concentration. To incorporate this dependence, we postulate the following linear relation:

$$t_D = t_D^0 c_P, \quad (21)$$

from which it is clear to see that the cell will almost certainly die if the PDGF concentration tends to zero. Since this happens at the final stages of the healing process, this effect can be seen as programmed cell death, that is apoptosis. For the (myo)fibroblasts, we assume that the survival rate is not determined by any of the concentrations TGF- β , PDGF or tPA, we set $t_D = t^f$.

2.2.4. Collagen synthesis and contact guidance

The orientation of the collagen influences the migration of fibroblasts and hence it is dealt with in this model. We use the formalism that was adopted by Cumming et al. (2010) who use a tensor approach in order to incorporate the orientation of the fiber. The advantage of this approach is that the density and orientation are incorporated. To this extent, we use the symmetric collagen tensor Ψ whose trace gives the collagen density

$$\rho_c = \text{tr}(\Psi) = \text{tr} \begin{pmatrix} \Psi_{xx} & \Psi_{xy} \\ \Psi_{xy} & \Psi_{yy} \end{pmatrix}. \quad (22)$$

Second, the eigenvectors of Ψ define the orientation of the fibers and the corresponding eigenvalues determine the dominance in the orientation of the fibers. The tensor representation then satisfies the following differential equation:

$$\frac{\partial \Psi}{\partial t} = (1 - \rho_f - \rho_c) \sum_{i=1}^{n_f} (k_2 n^i + k_1 (1 - n^i)) \mathbf{g}_i \mathbf{g}_i^T \cdot \mathbb{I}_c^i(\mathbf{x}). \quad (23)$$

Here $\mathbb{I}_c^i(\mathbf{x})$ denotes the indicator function, which is defined by

$$\mathbb{I}_c^i(\mathbf{x}) = \begin{cases} 1, & \mathbf{x} \in \Omega_c^i(t), \\ 0, & \mathbf{x} \notin \Omega_c^i(t). \end{cases} \quad (24)$$

Here $\Omega_c^i(t)$ denotes the region occupied by fibroblast i . Furthermore, \mathbf{g}_i represents the normalised migration vector of fibroblast i . Note that the above differential equation contains a summation over all fibroblasts. Only the fibroblasts are able to produce collagen and to adjust its orientation. Using the trace of the collagen tensor, one can prove that $\rho_c = 1 - \rho_f$ is a stable solution.

As an initial condition, we use isotropic collagen in the undamaged tissue, where we arrive at the following initial condition:

$$\Psi(0) = \frac{1}{2} \begin{pmatrix} \rho_c^0 & 0 \\ 0 & \rho_c^0 \end{pmatrix}. \quad (25)$$

In the initial wound area, we assume that there is no collagen.

The migration of the fibroblasts is influenced by the orientation of the collagen, and therewith we enrich the equation of migration of the (myo)fibroblasts to

$$d\mathbf{x}_i^f(t) = v_i^f \gamma_f (1 - n^i) ((1 - \rho_c) I + \Psi) \frac{\nabla c_\beta(\mathbf{x}_i^f(t))}{1 + \|\nabla c_\beta(\mathbf{x}_i^f(t))\|} dt + \sqrt{2D_f} d\mathbf{W}(t), \quad (26)$$

where I denotes the identity tensor.

2.2.5. The mechanical model

We consider the traction forces that are exerted by the (myo)fibroblasts which causes deformation of the tissue. To calculate this deformation, we solve

$$\begin{cases} \nabla \cdot \sigma + \mathbf{F} = \mathbf{0}, & \text{in } \Omega, \\ \tau \cdot (\sigma \cdot \mathbf{n}) = 0, \mathbf{u} \cdot \mathbf{n} = 0, & \text{in } \partial\Omega_1, \\ \sigma \cdot \mathbf{n} + \mathbf{K}\mathbf{u} = 0, & \text{on } \partial\Omega_2. \end{cases} \quad (27)$$

Here σ denotes the stress tensor. We use Hooke's Law for the relation between stress and strain. The forces exerted by the fibroblasts are represented by \mathbf{F} . Further \mathbf{u} denotes the displacement. The forces are decomposed into a temporary and a plastic part, that is $\mathbf{F} = \mathbf{F}_t + \mathbf{F}_p$. The temporary forces represent the actual traction forces exerted by the (myo)fibroblasts. The plastic forces are a consequence of the shortening of the collagen strings by the myofibroblasts. First, we deal with the temporary forces before the plastic forces are dealt with. We use the formalism proposed in Vermolen and Gefen (2015), where the cell boundary is divided into a set of meshpoints that are connected by line-segments in the present two dimensional setting. Over each line segment with

length $\Delta\Gamma_j$, a point force is introduced which works on the centre of the line-segment considered in the normal direction away from the cell centre. Let the number of (myo)fibroblasts be given by n_f and let the number of nodes on the cell boundary be given by n_b , then we have for all point forces

$$\mathbf{F}_t = \sum_{i=1}^{n_f} \sum_{j=1}^{n_b} P(t, \mathbf{x}_j) \mathbf{n}(\mathbf{x}_j) \delta(\mathbf{x} - \mathbf{x}_j) \Delta\Gamma_j. \quad (28)$$

Here \mathbf{n} denotes the unit normal vector directed out of the extracellular matrix, hence it is directed into the cell. Since the polygonal approximation of the cell warrants a piecewise smoothness, and since the force is assumed to be integrable, it follows that letting $\Delta\Gamma_j \rightarrow 0$ or $n_b \rightarrow 0$ makes the above expression tends to the following integral:

$$\mathbf{F}_t = \sum_{i=1}^{n_f} \mathbf{F}_t^i = \sum_{i=1}^{n_f} \int_{\partial\Omega_i} P(t, \mathbf{x}_s) \mathbf{n}(\mathbf{x}_s) \delta(\mathbf{x} - \mathbf{x}_s) d\Gamma_s. \quad (29)$$

Note that this representation of the force is similar to the treatment within the immerse boundary method from fluid dynamics. This relation was also developed in Vermolen and Gefen (2015), and there this approach was shown to be consistent with the case of treating cells as holes in the domain of computation where a forcing boundary condition is applied. The plastic forces are a result of shortening of collagen chains by the myofibroblasts. To this extent, we divide the domain into triangular subdomains (elements) and in each triangular element, we assign a forcing over the boundary that acts as the plastic force. The approach is similar to the treatment of the temporary forces, except now we apply the forcing over triangular control volumes instead of over cells. Let n_e be the total number of triangular elements, then

$$\mathbf{F}_p = \sum_{e=1}^{n_e} \mathbf{F}_p^e, \quad (30)$$

where \mathbf{F}_p^e represents the plastic force over triangular element e , given by the following sum over the sides:

$$\mathbf{F}_p^e = \sum_{p=1}^3 Q(\tau_e) \mathbf{n}(\mathbf{x}_p^e) \delta(\mathbf{x} - \mathbf{x}_p^e) \Delta l_p, \quad (31)$$

where \mathbf{x}_p^e , Q and Δl_p , respectively, represent the coordinates of the midpoint of side p , the magnitude of the traction force on this midpoint and the length of side p . The traction force Q depends on the amount of effective time, denoted by τ_e , that this element is occupied by a myofibroblast. To this extent, we treat τ_e as a timer which is incremented if element e is occupied by a myofibroblast. In order to be consistent in the dimensions of the cells and elements, the increment is determined by the actual fraction of the area of the element that is occupied by myofibroblasts. To this extent, we use

$$\frac{d\tau_e}{dt} = \frac{\mathcal{A}(\Omega_e(t) \cap (\cup_i \Omega_f^i(t)))}{\mathcal{A}(\Omega_e(t))}, \quad \tau_e(0) = 0, \quad (32)$$

where $\mathcal{A}(\cdot)$ denotes the area. The traction force exerted on the element is assumed to proceed via the shortening reaction of the polymeric chains. This chemical reaction is assumed to be of first order. We further assume that the traction force is linearly related to the chemical shortening of the chains and hence we assert

$$\frac{\partial Q(\tau)}{\partial \tau} = \alpha_\tau \rho_c (Q_{max} - Q(\tau)), \quad Q(0) = 0. \quad (33)$$

Here Q_{max} represents the maximum traction force. The existence of a maximum traction force is reasonable since there is always a minimal bond length away from zero for the polymeric chains. As a result of all the traction forces (both plastic and temporary), the

domain of computation deforms and thereby the wound area decreases and by this phenomenon wound contraction is modeled.

3. Numerical solution method

The system of mathematical relations represents a complicated system with partial differential equations and stochastic processes. All partial differential equations are solved using the standard Galerkin finite-element method. This holds for all concentrations as well as for the mechanical model. Bearing in mind that the finite-element method is a standard technique, we will explain the issues that are non-standard in our approach. As a result of the traction forces the domain of computation contracts. Further, the numerical treatment of the stochastic differential equations for cellular migration is presented. First, we present the numerical treatment of the partial differential equations for the concentrations of the chemical entities. Subsequently, the treatment of cellular migration is described and finally the numerical evaluation of the cell traction is introduced.

3.1. The chemical entities

The chemical entities such as concentration of the growth factors, but also the tissue identifiers, obey transport-reaction equations. For the sake of efficiency, we only present the treatment in a generic way. Let $\phi = \phi(t, \mathbf{x})$ be a continuous field parameter, such as a concentration, then we have

$$\frac{\partial \phi}{\partial t} + \nabla \cdot \mathbf{J} = f(t, \mathbf{x}, \phi), \quad (34)$$

subject to initial and boundary conditions. Here \mathbf{J} and f , respectively, represent a flux and reactive term. As a result of the traction forces exerted by the cells, there will be a displacement field over the domain of computation. Let $\mathbf{u}(t, \mathbf{x})$ denote the displacement vector on coordinates \mathbf{x} in the reference frame, then we denote $\mathbf{v} = \frac{d}{dt}\mathbf{u}$ as the displacement velocity. Then the dynamics of the movement of the coordinates is incorporated in the above equation by the passive convection term $\nabla \cdot (\mathbf{v}\phi)$

$$\frac{\partial \phi}{\partial t} + \nabla \cdot (\mathbf{v}\phi) + \nabla \cdot \mathbf{J} = f(t, \mathbf{x}, \phi). \quad (35)$$

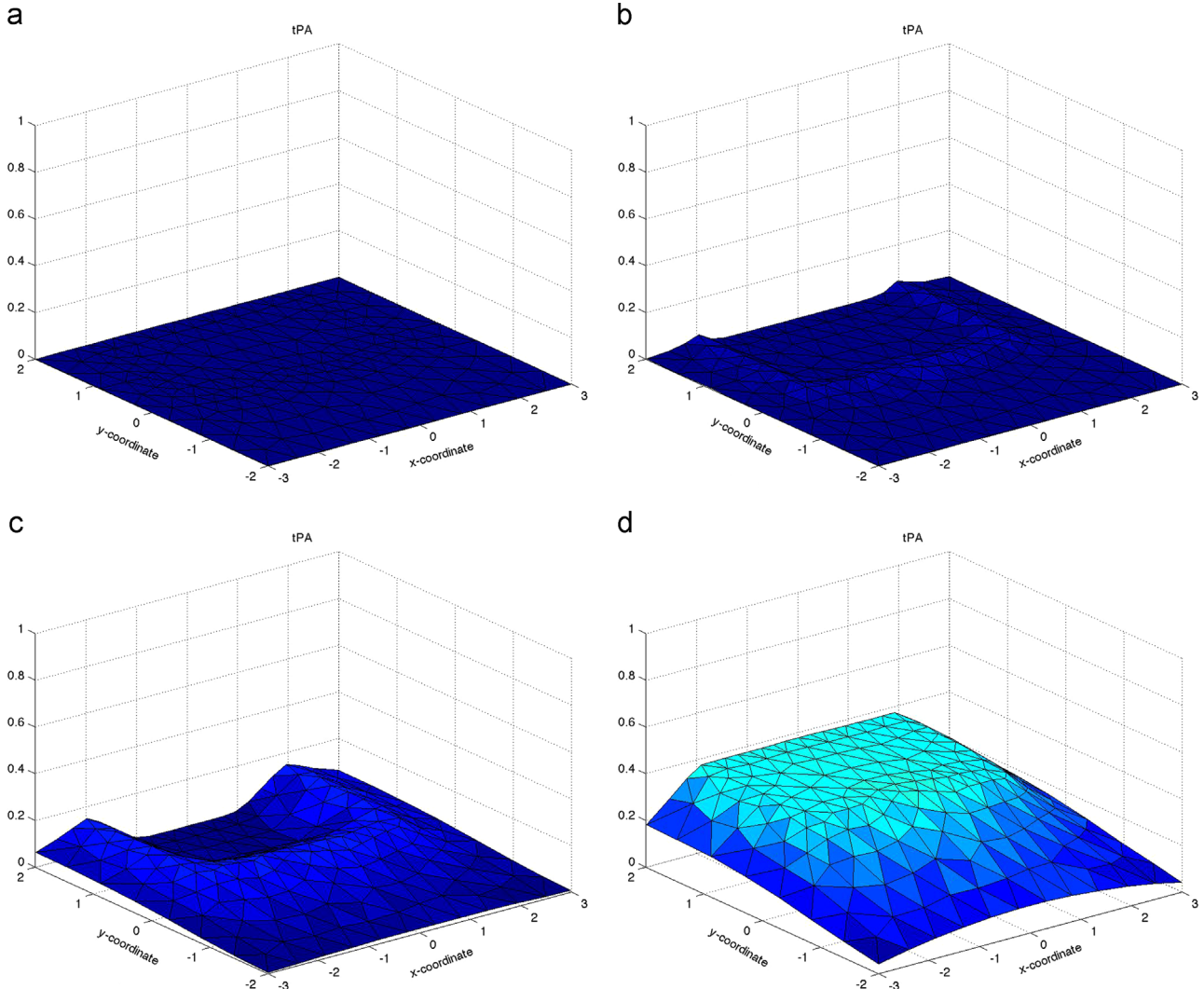


Fig. 1. Some snapshots of the tPA-profile at consecutive times. We show the results for $t = 0$, $t = 0.1$, $t = 1$ and $t = 24$ h.

Applying the Product Rule for differentiation and the total derivative (material derivative) for ϕ , given by

$$\frac{d\phi}{dt} = \frac{\partial \phi}{\partial t} + \mathbf{v} \cdot \nabla \phi,$$

gives

$$\frac{d\phi}{dt} + \phi(\nabla \cdot \mathbf{v}) + \nabla \cdot \mathbf{J} = f(t, \mathbf{x}, \phi), \quad (36)$$

Since we use the Galerkin finite-element method to solve the partial differential equations, the above equation is multiplied by a test function, $\varphi(\mathbf{x})$, that satisfies certain requirements regarding integrability ($\varphi \in H^1(\Omega)$) after integration by parts. Subsequently, the equation is integrated over the domain of computation Ω_t , which depends on time t , to obtain

$$\int_{\Omega_t} \varphi \left(\frac{d\phi}{dt} + \phi \nabla \cdot \mathbf{v} + \nabla \cdot \mathbf{J} \right) d\Omega = \int_{\Omega_t} \varphi f d\Omega. \quad (37)$$

Using the Product Rule for the total derivative and the transport property of finite-element functions $\frac{d\varphi}{dt} = 0$ (see Dziuk and Elliott (2007)) and using

$$\frac{d}{dt} [\phi\varphi] = \frac{\partial}{\partial t} [\phi\varphi] + \nabla \cdot [\mathbf{v}\phi\varphi] - \phi\varphi(\nabla \cdot \mathbf{v}),$$

gives

$$\int_{\Omega_t} \frac{\partial(\phi\varphi)}{\partial t} + \nabla \cdot [\phi\varphi\mathbf{v}] + \phi\nabla \cdot \mathbf{J} d\Omega = \int_{\Omega_t} \varphi f d\Omega. \quad (38)$$

Finally, we apply Gauss' Theorem on the second term and we integrate the third term by parts, to obtain

$$\int_{\Omega_t} \left(\frac{\partial(\phi\varphi)}{\partial t} - \nabla\varphi \cdot \mathbf{J} \right) d\Omega + \int_{\partial\Omega_t} \varphi (\mathbf{J} \cdot \mathbf{n} - \phi\mathbf{v} \cdot \mathbf{n}) d\Gamma = \int_{\Omega_t} \varphi f d\Omega. \quad (39)$$

Application of the Reynold Transport Theorem, gives

$$\frac{d}{dt} \int_{\Omega_t} \phi\varphi d\Omega - \int_{\Omega_t} \nabla\varphi \cdot \mathbf{J} d\Omega + \int_{\partial\Omega_t} \varphi \mathbf{J} \cdot \mathbf{n} d\Gamma = \int_{\Omega_t} \varphi f d\Omega. \quad (40)$$

The boundary integral is further processed using the boundary conditions. In the finite-element method, all solutions are represented in terms of linear combinations of basis functions where the weights depend on time. The resulting system of ordinary differential equations are integrated using the backward Euler method whenever the equations are linear. If the case of nonlinear equations, the IMEX method is used for the temporal integration.

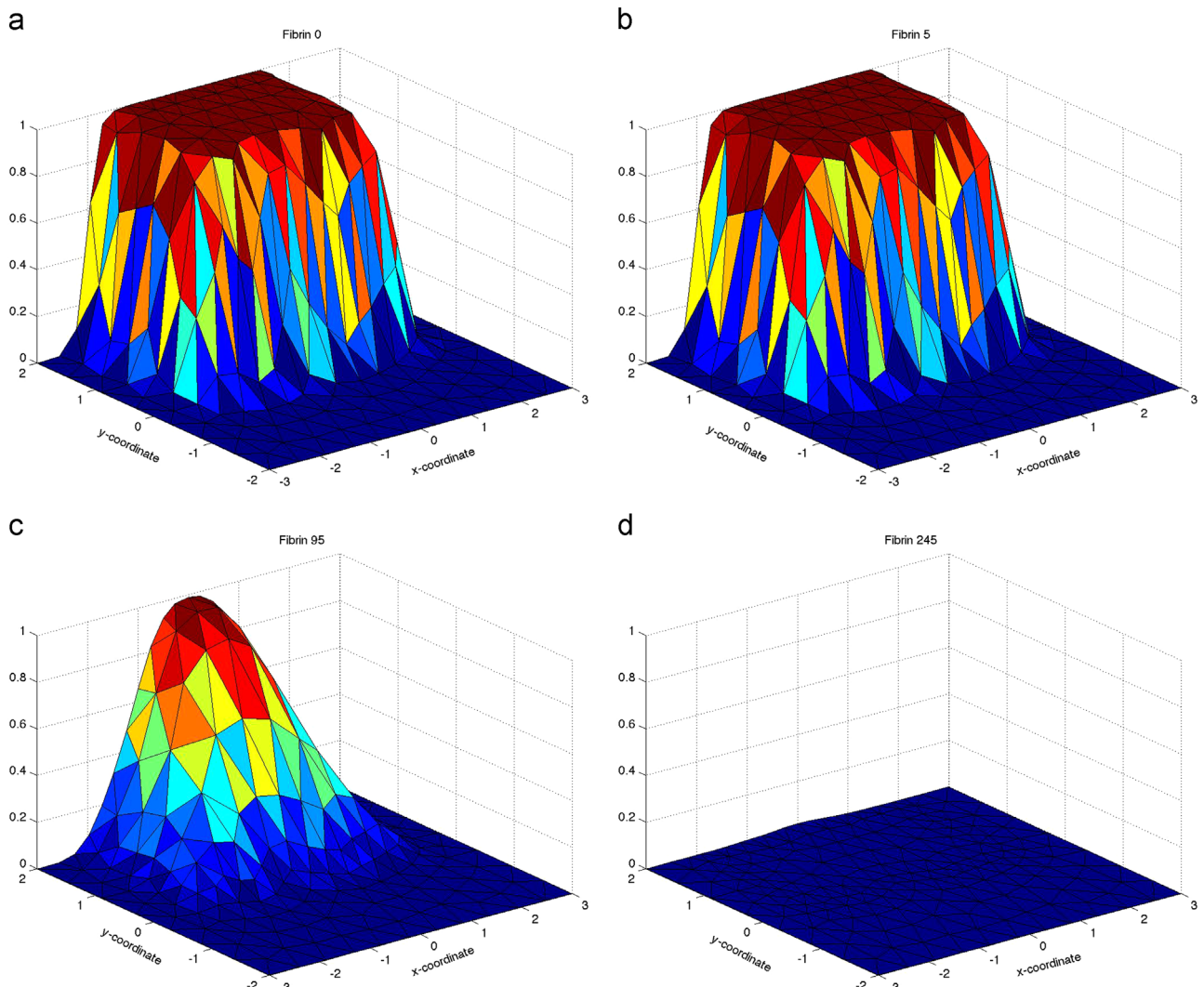


Fig. 2. Some snapshots of the fibrin-profile at consecutive times. We show the results for $t=0$, $t=1$, $t=2$ and $t=5$ h.

3.2. The mechanical balance

The equations for the mechanical balance are solved analogously using standard methods. Only the treatment of the cell traction forces will be summarised. After integration by parts and using the boundary conditions, the weak form of Eqs. (27) is derived. Since this step is standard, we do not repeat this. We will only focus on the treatment of the cell traction forces in the weak formulation. In order to maintain efficiency, the cell boundary is simplified to a square with sides parallel to the horizontal and vertical axes. Having a cell with radius R , we maintain its area and set the four centers of the sides for cell i with centre \mathbf{x}_i^f on $(x_i^f + L/2, y_i^f)$, $(x_i^f, y_i^f + L/2)$, $(x_i^f - L/2, y_i^f)$ and $(x_i^f, y_i^f - L/2)$. Here L is chosen such that $L^2 = \pi R^2$, if R is the cell radius. Using the integral property of the Dirac Delta Distribution, with respect to cell j , the weak form of the temporary traction forces is given by

$$\int_{\Omega_t} \varphi_i \mathbf{F}_t^i d\Omega = \int_{\Omega_t} \varphi_i \left(P(t, (x_j^f + L/2, y_j^f)) \varphi_i(x_j^f + L/2, y_j^f) - P(t, (x_j^f - L/2, y_j^f)) \varphi_i(x_j^f - L/2, y_j^f) \right) \\ = -L \left(P(t, (x_j^f, y_j^f + L/2)) \varphi_i(x_j^f, y_j^f + L/2) - P(t, (x_j^f, y_j^f - L/2)) \varphi_i(x_j^f, y_j^f - L/2) \right) \quad (41)$$

The second type of contractile forces, the plastic tractions over

element e , are evaluated by

$$\int_{\Omega_t} \varphi_i \mathbf{F}_p^e d\Omega = \int_{\Omega_t} \varphi_i \sum_{p=1}^3 Q(\tau_e) \mathbf{n}(\mathbf{x}_p^e) \delta(\mathbf{x} - \mathbf{x}_p^e) \Delta l_p d\Omega \\ = \sum_{p=1}^3 P(\tau_e) \mathbf{n}(\mathbf{x}_p^e) \varphi(\mathbf{x}_p^e) \Delta l_p. \quad (42)$$

3.3. The cell migration

To solve the stochastic differential equation for the cell displacement, see (26), we use the Euler–Maruyama method. We explain the algorithm for the migration of fibroblasts, then the migration of leukocytes is treated analogously. Let $\tilde{\mathbf{x}}_i^f(t_k)$ denote the numerical approximation of the position $\mathbf{x}_i^f(t_k)$ at time t_k , then we get

$$\tilde{\mathbf{x}}_i^f(t_{k+1}) = \tilde{\mathbf{x}}_i^f(t_k) + \mathbf{v}_i^f(t_k) \gamma_f (1 - n^i(t_k)) ((1 - \rho_c(t_k)) I \\ + \Psi(t_k, \tilde{\mathbf{x}}_i^f(t_k))) \frac{\nabla c_\beta(t_k, \tilde{\mathbf{x}}_i^f(t_k))}{1 + \|\nabla c_\beta(t_k, \tilde{\mathbf{x}}_i^f(t_k))\|} \Delta t + \mathbf{v}_{con}(t_k) \Delta t \\ + (\mathbf{u}(t_{k+1}, \tilde{\mathbf{x}}_i^f(t_{k+1})) - \mathbf{u}(t_k, \tilde{\mathbf{x}}_i^f(t_k))) + \sqrt{2D_f} \Delta \mathbf{W}, \quad (43)$$

where \mathbf{v}_{con} denotes the velocity as a result of mechanical impingement. See [Vermolen and Gefen \(2012\)](#) for more details

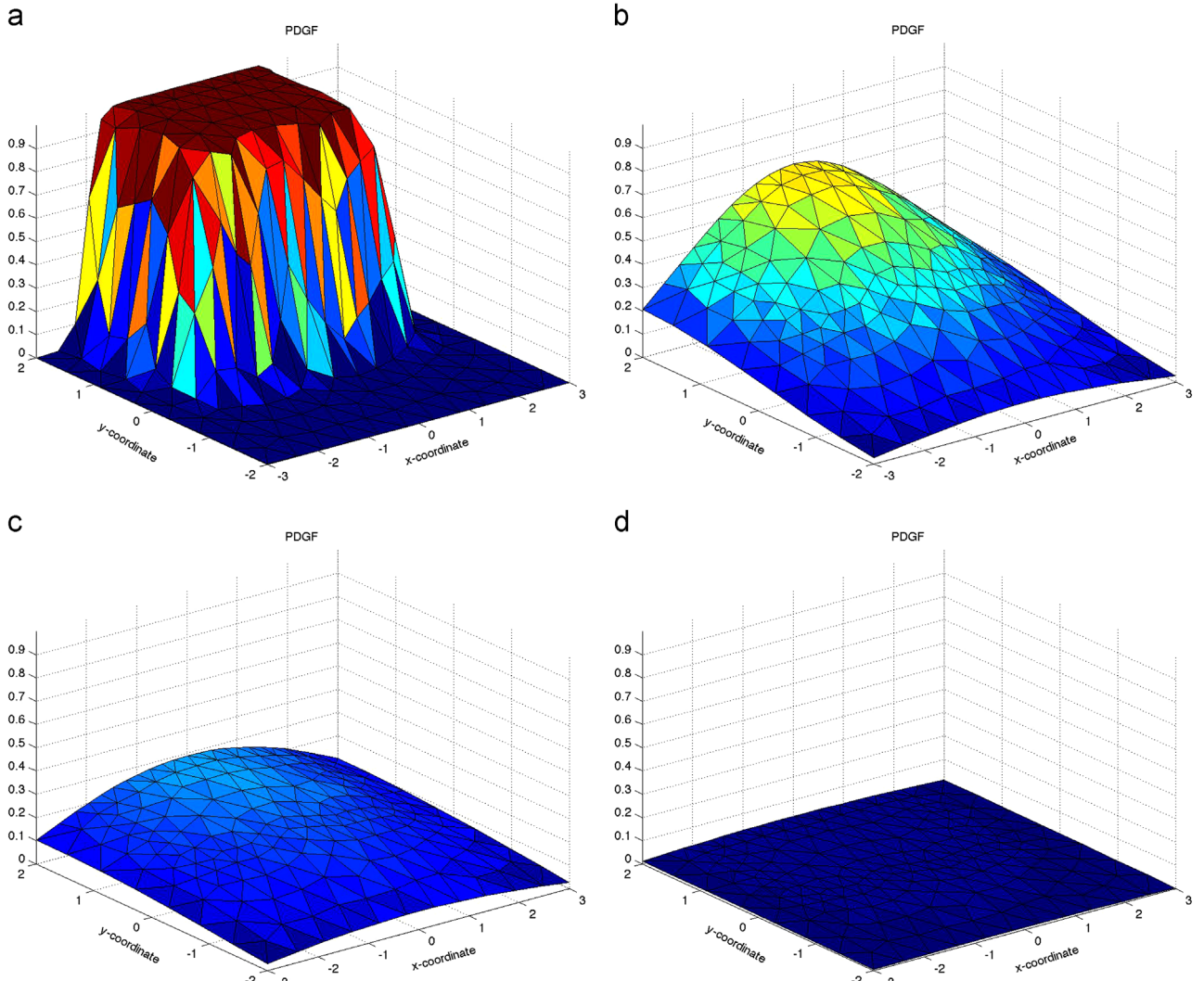


Fig. 3. Some snapshots of the fibrin-profile at consecutive times. We show the results for $t = 0:1$, $t = 2$ and $t = 5$ h.

regarding this contribution. Further, the vectorial stochastic variable $\Delta\mathbf{W}(t_k)$ contains a vector with two or three realisations from a normal distribution as follows:

$$\Delta\mathbf{W} = [\Delta W_x \quad \Delta W_y]^T, \quad (44)$$

for the two-dimensional case, where $\Delta W_x, \Delta W_y \sim \mathcal{N}(0, \Delta t)$ are two independent realisations from the normal distribution with zero mean and variance Δt . Further, mechanical drag has been taken into account by the displacement vector over a time-step Δt . Note that the displacements are obtained by mapping the solution of the displacement from mechanical equilibrium to the position of the centres of the cells. Since we use linear basis functions on the triangular finite-element mesh, we use linear interpolation based on the finite-element basis functions. The time-stepping was chosen such that cells do not migrate more than one-fourth of their diameter. This warrants a sufficiently small time-step such that numerical stability is obtained.

4. Numerical simulation results

First we give a basic simulation in which we present the quantities that are computed in the model. The default values have been listed in Appendix A. Subsequently, we present some results where the values of parameters are varied.

4.1. The basis run

We start with the presentation of the continuous variables, and subsequently we consider the cells. In Fig. 1, the tPA concentration is plotted at consecutive times. It can be seen that there is gradual build-up from the wound edge and that the tPA moves into the wound where it will be able to decay the fibrin that is present originally. This behavior is natural since tPA is secreted by the endothelial cells that build up the small blood vessels around the periphery of the wound. Furthermore, the concentration is somewhat lower on the boundary of the computational domain since it is assumed that far away from the wound, the level of tPA is negligible.

The decay of the fibrin by the tPA can be seen in Fig. 2, where several snapshots at consecutive times are presented for the fibrin network density. The decay proceeds approximately within 5 h. It can be seen that the decay first starts at the boundary of the wound, from which the front of decay migrates deeper into the wound. The evolution of the profile of the platelet derived growth-factor can be seen in Fig. 3, where it can be seen that the initial profile is characterised by a large value in the vicinity of the wound as a result of secretion by the platelets that were positioned in the wound immediately post-wounding. Subsequently, the PDGF diffuses away from the wound into the deeper tissue. The gradient of this growth factor attracts the leukocytes towards

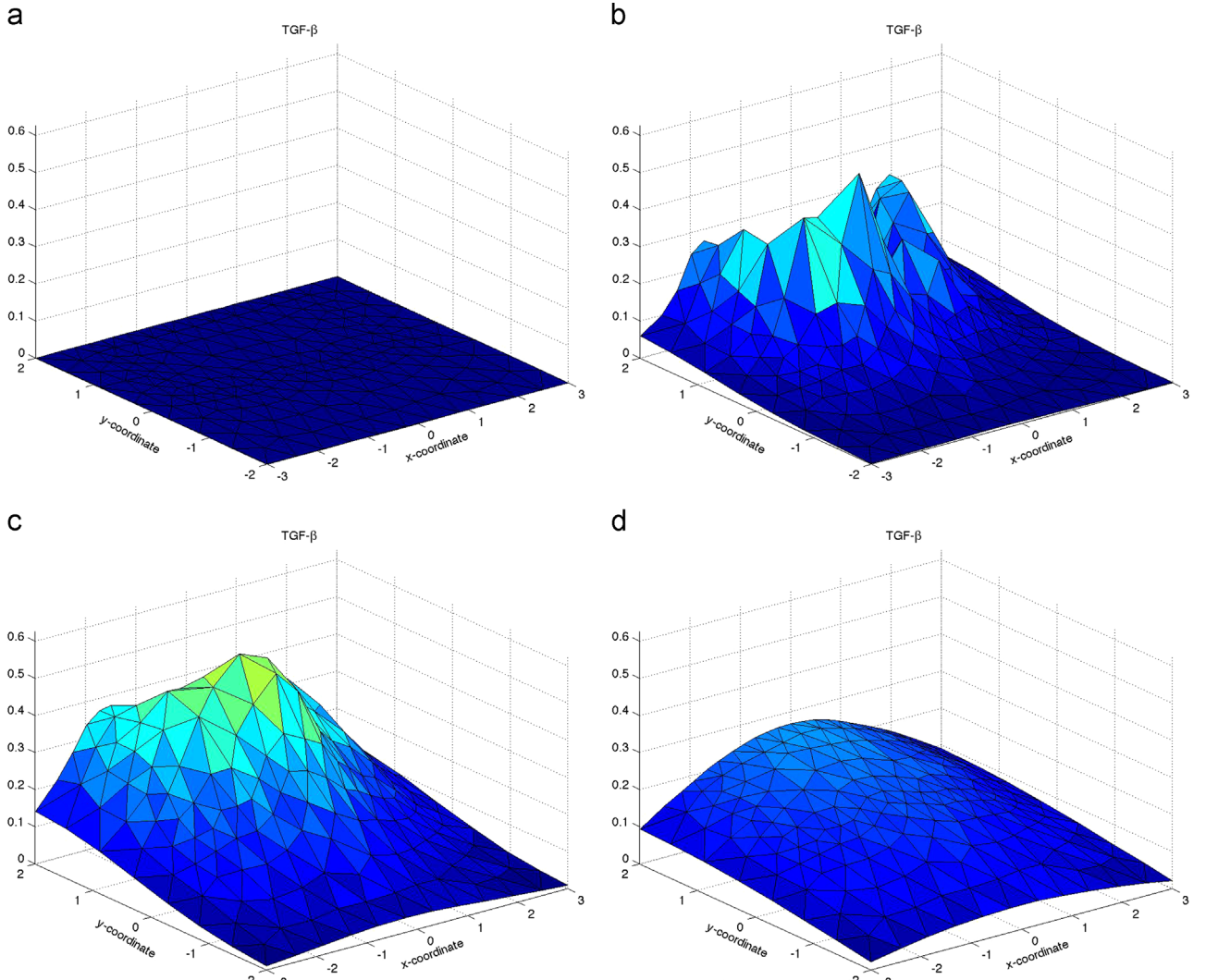


Fig. 4. Some snapshots of the TGF-profile at consecutive times. We show the results for $t=0, t=1, t=2$ and $t=5$ h.

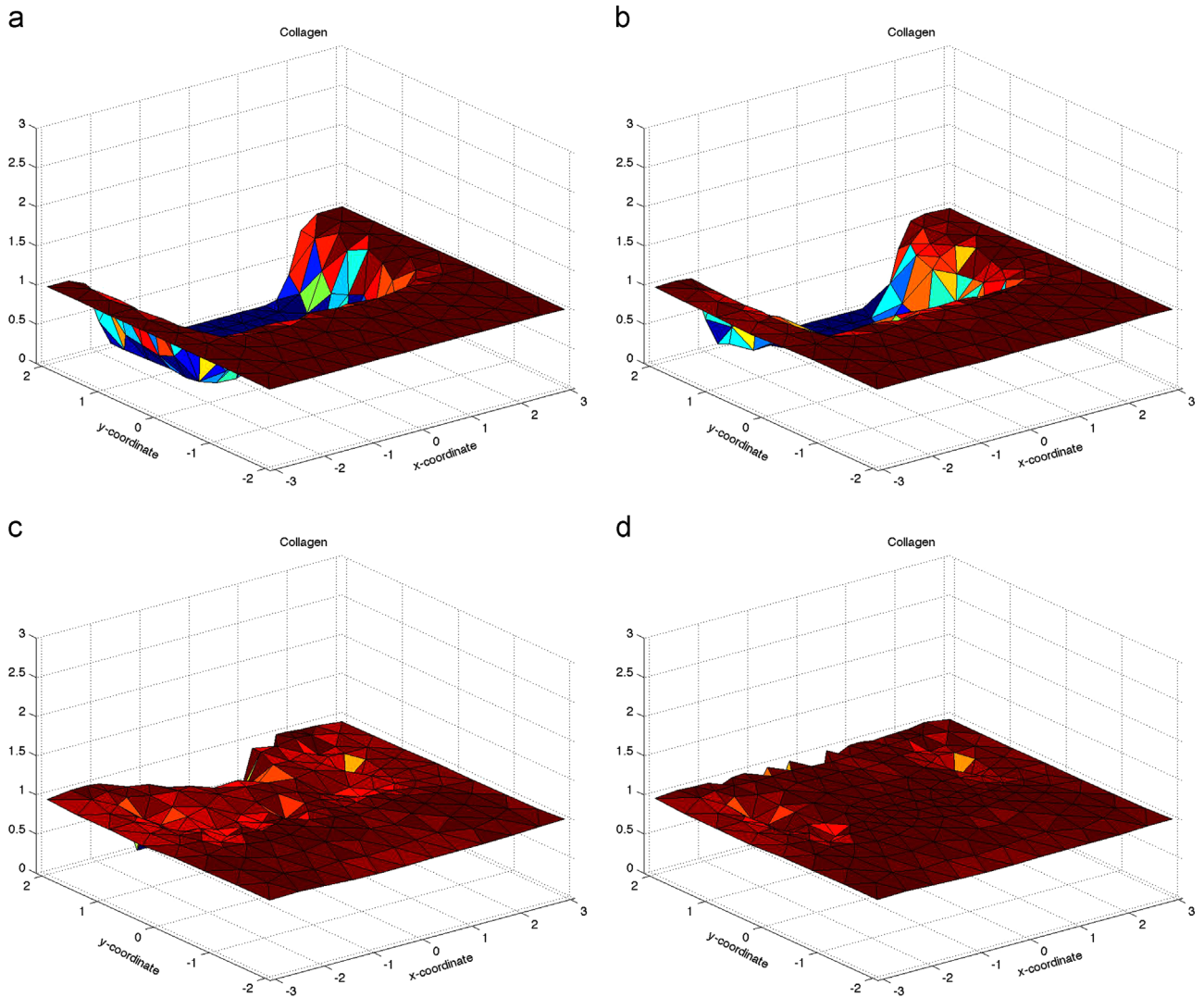


Fig. 5. Some snapshots of the collagen-profile at consecutive times. We show the results for $t=0$, $t=2$, $t=4$ and $t=24$ h.

the wound centre. Furthermore, the actual value of the PDGF concentration influences the number of leukocytes that actually leave the surrounding small blood vessels.

As soon as the PDGF profile builds up, leukocytes enter the wound area. The leukocytes secrete TGF- β , which is the main attractant of the fibroblasts. Several snapshots are presented in Fig. 4, where it can be seen that the discrete character regarding the cells, gives a spiky behavior at the early stages. As the ingress of leukocytes proceeds, the amount of TGF- β increases, as well due to diffusion, the profile gets a smoother character. In the very long run, the concentration decays down to zero.

As soon as the fibroblasts enter the wound scene, they start depositing collagen. The amount of collagen is determined by the trace of the collagen tensor. Since the fibroblasts are treated as individual cells, and since the collagen is not subject to diffusion, the profiles exhibit a discontinuous, spiky behaviour over space, even at larger times, see Fig. 5.

Subsequently, we show several snapshots at consecutive times for the leukocytes (immune cells) and fibroblasts that are entering the wound region in Fig. 6. The fibroblasts produce collagen that is oriented according to their migration velocity vector. In Fig. 6, the crosses with lines of equal length represent regions without any preferential collagen orientation (hence the orientation is isotropic there). Regions with just one relatively long line correspond to

regions where new collagen has been deposited by the fibroblasts. Here the orientation is non-isotropic. The direction of the lines represent the preferential orientation as the largest eigenvalue in the collagen orientation tensor. The red circles indicate the positions of the immune cells, which enter the wound as a result of the gradient of platelet derived growth factor. The blue circles indicate the positions of the fibroblasts, which are lured into the wound area by the gradient of the TGF- β that is secreted by the immune cells. It can be seen clearly that during the early stages there is front of leukocytes entering the wound section and that this front is followed by the ingress of fibroblasts. It can also be seen that the wound area indicated by the red line contracts during the process. In the longer run, the leukocytes and the fibroblasts will die to small numbers at the very end of the simulation. It can be seen that the new collagen that has been deposited by the fibroblasts possesses an oriented structure towards the centre of the wound according to the mean ingress of fibroblasts.

4.2. Parameter variation

Since one of the most problematic issues regarding severe burns or deep wounds is the permanent contraction of the wound. This permanent contraction often gives rise to reduced patient mobility and this is the reason why we consider the wound area

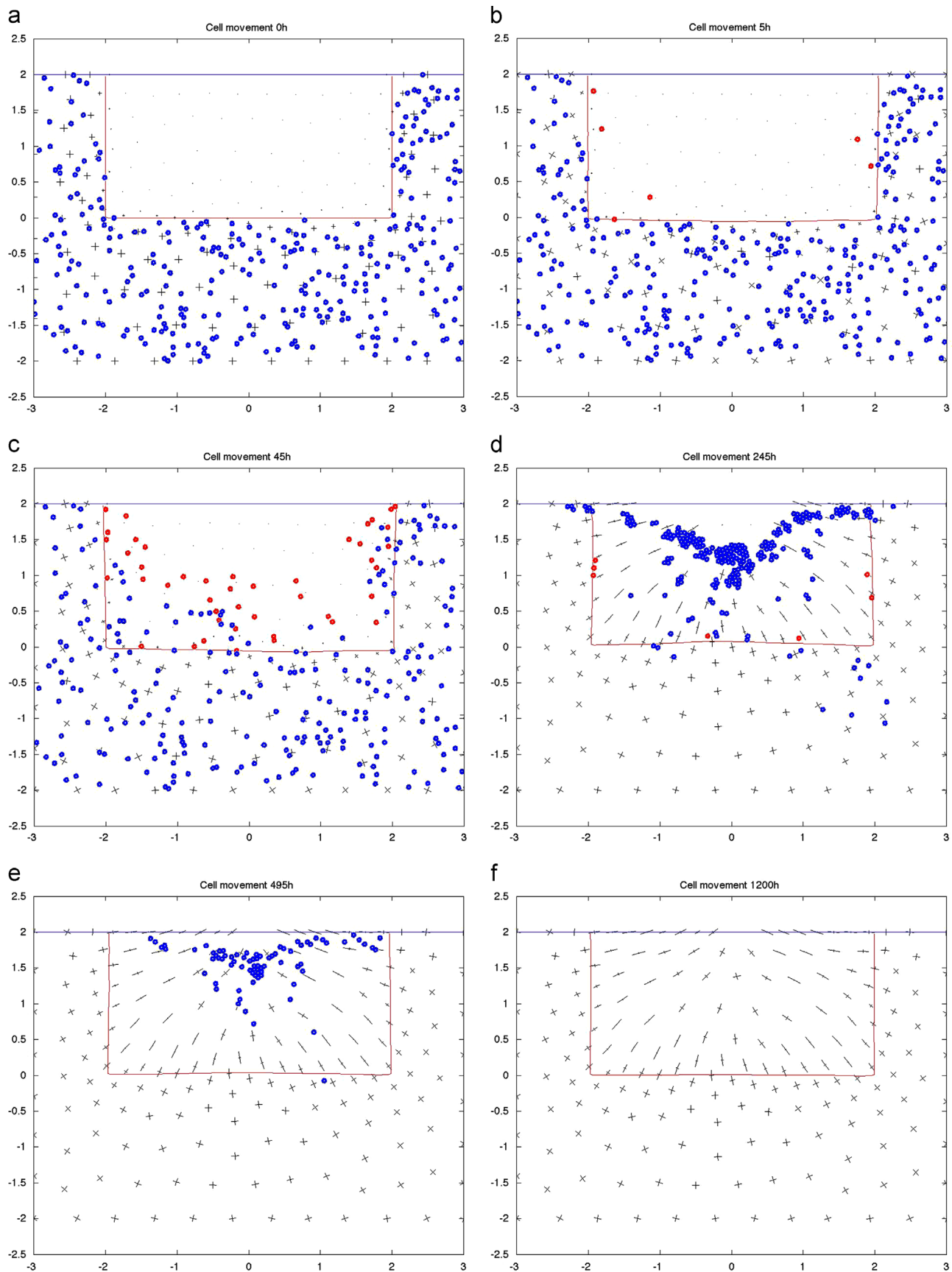


Fig. 6. Some snapshots of the cells (leukocytes in red and fibroblasts in blue) at consecutive times. The wound area is depicted by the red line. Further, the collagen orientation is displayed by the black lines. We show the results for $t = 0$, $t = 0:2$, $t = 1$, $t = 5$, $t = 10$ and $t = 24$ h. (For interpretation of the references to color in this figure legend, the reader is referred to the web version of this article.)

versus time. In particular, we are interested in the contraction for larger times, that is, the permanent reduction of the wound area. In Fig. 7, we show the wound area versus time.

The stochastic parts in the model necessitate us to present several runs for each parameter value. For each parameter value we completed four runs. From these runs, we estimate the mean value of the final contraction area. Although a rigorous statistical analysis needs the determination of the interval of confidence for the mean values of output-parameters, this has not yet been done at this stage of the research. An evaluation of the curves shows that at the very early stages, the wound expands a little, subsequently contracts, and finally expands up to its final configuration. The first expansion phase follows from the fact that first the fibroblasts are located outside the wound, hence in the undamaged tissue. Since they are already pulling at this stage, the wound edge is drawn away from the wound centre. Subsequently, the fibroblasts migrate into the wound, where they continue pulling and start depositing collagen. Therewith the wound edge is drawn towards the wound centre and the contraction phase starts. During this phase, they also shorten the polymeric chains of the

collagen molecules, whereby the material deforms plastically. At the final stages, the fibroblasts die, and hence their pulling forces are no longer there, despite of this, yet the plastic forces remain and therewith the material stays deformed in the long run. Therefore, the wound area is characterised by a final contraction. Reducing the cell traction force, results into lower deformations and hence into lower wound area reductions. Decreasing the ratio between the cell traction and the permanent contraction (hence by decreasing the permanent traction forces), the final contraction decreases.

Since the crucial quantity is the final contraction that the patient experiences, we plot the final relative decrease of area versus α_T and the maximum migration speed of the leukocytes. The parameter α_T represents a measure of the rate at which the collagen molecules are shortened by the fibroblasts. The results have been plotted in Fig. 8. It can be seen that for low values of α_T , the amount of contraction climbs up to a maximum. The reason is that for larger α_T -values the force is able to increase up to a large value so that the wound gets contracted. An interesting behaviour seems to take place if the value of α_T increases even more. Then the amount of contraction drops. This is probably caused by the fact that the fibroblasts immediately reach shorten the chains, also if they are outside the wound area. Then over all places there is a contractile force which levels all the contributions so that the net displacement of the wound boundary remains relatively small. Next, we consider the influence of the leukocyte maximum velocity component as a result of chemotaxis. It can be seen that as the leukocytes move more quickly, the final amount of contraction stays smaller. The reason is that if the leukocytes are deeper in the wound then the driving force for the fibroblasts to enter deeper into the wound area will be smaller due to smaller gradients. Hence the amount of contraction decreases. From this result, it can be seen that if the leukocytes are paralysed then the amount of final contraction is larger. It is hence important that the immune system functions well. Loss of leukocyte motility could be caused by diseases like diabetes or AIDS.

5. Discussion and conclusions

A multi-agent cell-based hybrid model that can be used to simulate the dynamics of the contracture of dermal wounds has been presented. The model takes into account the ingress of leukocytes, fibroblasts, and the regeneration of collagen in which its

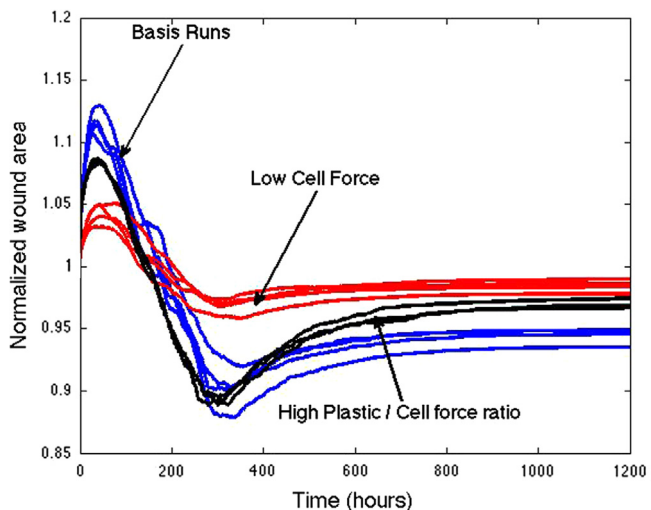


Fig. 7. The wound area for the basis-run, as well as for two other cases in which the cellular traction force is reduced to one-third as well as the ratio between the plastic forces and temporary forces has been decreased by 1/2.5. For each parameter value, several runs have been shown.

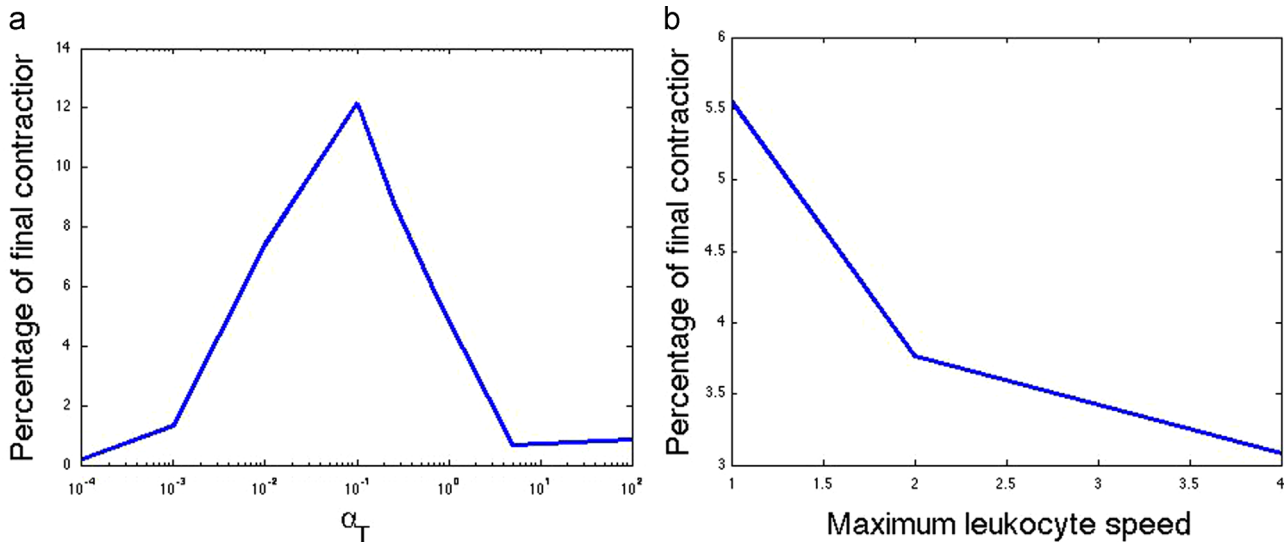


Fig. 8. The amount of final contraction given in percentage as a function of the α_T -parameter (left) and as a function of the maximum leukocyte migration speed (right).

orientation is taken into account. The model is capable of predicting the various subsequent phases that take place during the formation of a wound contracture. First, the wound area expands as a result of fibroblasts that are outside the wound area where they exert traction forces. Subsequently, the fibroblasts migrate into the wound where they keep on exerting the contractile forces, which makes the wound area decrease over time. Further, the fibroblasts will change the collagen in the tissue where the polymeric chain are shortened whereby permanent traction forces remain. The last-mentioned mechanism is responsible for the occurrence of a permanent contraction. Besides the ingress of fibroblasts, the immune response system is taken into account. The platelet derived growth factor triggers the immune system response in the sense that the concentration determines the number of leukocytes leaving the blood vessels. This effect has been incorporated by the introduction of the probability of occurrence of leukocytes over the wound boundary. Furthermore, the leukocytes are directed towards the higher levels of platelet derived growth factor. These issues all have been taken care of in the present modelling. The model is capable to investigate the influence of the various parameters, such as the leukocyte motility. It has been found that the final contracture is less severe for lower values of maximum leukocyte migration speeds. Furthermore, the impact of the chain shortening rate has been evaluated on the amount of final contracture. The effect is non-monotonic notably due to the overall shortening of the chains at all location when the shortening rate is extremely large. Since the model takes into account that the shortening takes place at a rate proportional to the collagen density, the traction forces are distributed rather homogeneously over the domain of computation, including the domain around the wound for extremely high rates of chain shortening. Further, the model contains several stochastic components, such as cell death and cell migration. This is the reason why for each case several runs have to be carried out. In order to decide whether the impact of a parameter is significant, a rigorous statistical hypothesis testing procedure needs to be carried out where intervals of confidence for the mean value of the final contraction percentage are determined. In this paper, we have chosen to use the amount of final contracture is taken since this parameter seems to be most important regarding the clinical appearance of the final contraction, which is mostly limiting to a patient's mobility. To our knowledge, the present model is the first cell-based model that links the immune response system to the occurrence of permanent contractions.

A future useful extension of the model is to link the present formalism to the model by Valero et al. (2015) to incorporate the fiber anisotropy into the mechanical balance.

Conflict of interest

All authors have no conflict of interest.

Acknowledgements

The authors are grateful for the financial support by the Dutch Burns Foundation under Project 12.103.

Appendix A. Supplementary data

Supplementary data associated with this paper can be found in the online version at <http://dx.doi.org/10.1016/j.jbiomech.2015.11.058>.

References

- Barocas, V.H., Tranquillo, R.T., 1997. An anisotropic biphasic theory of tissue-equivalent mechanics: the interplay among cell traction, fibrillar network deformation, fibril alignment, and cell contact guidance. *J. Biomech. Eng.* 119 (2), 137–145.
- Barrantes, S., Stojadinovic, O., Golinko, M.S., Brem, H., Tomic-Canic, M., 2008. Growth factors and cytokines in wound healing. *Wound Repair Regener.* 16, 585–601.
- Cesarman-Maus, G., Hajjar, K.A., 2005. Molecular mechanisms of fibrolysis. *Brit. J. Haematol.* 129, 307–321.
- Clark, R.A., 2014. Basic biology to tissue engineering. In: Lanza, R., Langer, R., Vacanti, J. (Eds.), *Wound Repair*, fourth edition Academic Press, Boston, pp. 1595–1617.
- Cumming, B.D., McElwain, D.L.S., Upton, Z., 2010. A mathematical model of wound healing and subsequent scarring. *J. R. Soc. Interface* 7, 19–34.
- Dallon, J.C., Sherratt, J.A., Maini, P.K., Ferguson, M., 2000. Biological implications of a discrete mathematical model for collagen deposition and alignment in dermal wound repair. *IMA J. Math. Appl. Med. Biol.* 17 (4), 379–393.
- Dallon, J.C., Sherratt, J., Maini, P.K., 1999. Mathematical modelling of extracellular matrix dynamics using discrete cells: fiber orientation and tissue regeneration. *J. Theoret. Biol.* 199 (4), 449–471.
- Dallon, J.C., Sherratt, J.A., Maini, P.K., 2001. Modelling the effects of transforming growth factor-beta on extracellular matrix alignment in dermal wound repair. *Wound Repair Regener.* 9 (4), 278–286.
- Deuel, T.F., Senior, R.M., Griffin, G.L., 1982. Chemotaxis of monocytes and neutrophils to platelet-derived growth factor. *J. Clin. Invest.* 69 (4), 1046–1049.
- Dziuk, G., Elliott, C.M., 2007. Finite elements on evolving surfaces. *IMA J. Numer. Anal.* 27 (2), 262–292.
- Ellis, I., Schor, S.L., 1996. Differential effects on TGF- β 1 on hyaluronan synthesis by fetal and adult skin fibroblasts: implication for cell migration and wound healing. *Exp. Cell Res.* 228, 326–333.
- Enoch, S., Leaper, D.J., 2008. Basic science of wound healing. *Surgery (Oxford)* 26 (2), 31–37.
- Hinz, B., 2006. Masters and servants of the force: the role of matrix adhesions in myofibroblast force perception and transmission. *Eur. J. Cell Biol.* 85 (3–4), 175–181.
- Javierre, E., Moreo, P., Doblaré, M., García-Aznar, J.M., 2009. Numerical modeling of a mechano-chemical theory for wound contraction analysis. *Int. J. Solids Struct.* 46 (20), 3597–3606.
- Marks, J.G., Miller, J.J., 2013. *Lookingbill and Marks' Principles of Dermatology*, fifth edition. Elsevier Saunders, Philadelphia, PA.
- McDougall, S., Dallon, J.C., Sherratt, J.A., Maini, P.K., 2006. Fibroblast migration and collagen deposition during dermal wound healing: mathematical modelling and clinical applications. *Philos. Trans. R. Soc. A: Math. Phys. Eng. Sci.* 364, 1385–1405.
- Murphy, K.E., Hall, C.L., Maini, P.K., McCue, S.W., McElwain, D.L., 2012. A fibrocontractive mechanochemical model of dermal wound closure incorporating realistic growth factor kinetics. *Bull. Math. Biol.* 74 (5), 1143–1170.
- Olsen, L., Sherratt, J.A., Maini, P.K., 1995. A mechanochemical model for adult dermal wound closure and the permanence of the contracted tissue displacement role. *J. Theoret. Biol.* 177, 113–128.
- Olsen, L., Sherratt, J.A., Maini, P.K., 1996. A mathematical model for fibroproliferative wound healing disorders. *Bull. Math. Biol.* 58 (4), 787–808.
- Olsen, L., Maini, P.K., Sherratt, J.A., Dallon, J.C., 1999. Mathematical modelling of anisotropy in fibrous connective tissue. *Math. Biosci.* 158 (2), 145–170.
- Postlethwaite, A.E., Keski-Oja, J., Moses, H.L., Kang, A.H., 1987. Stimulation of chemotactic migration of human fibroblasts by TGF- β . *J. Exp. Med.* 165, 251–256.
- Postlethwaite, A.E., Seyer, J.M., Kang, A.H., 1978. Chemotactic attraction of human fibroblasts to type I, II and III collagens and collagen-derived peptides. *Proc. Natl. Acad. Sci. USA* 75 (2), 871–875.
- Pierce, G.F., Mustoe, T.A., Altrock, B.W., Deuel, T.F., Thomason, A., 1991. Role of platelet-derived growth factor in wound healing. *J. Cell. Biochem.* 45 (4), 319–326.
- Seppä, H., Grotendorst, G., Seppä, S., Schiffmann, E., Martin, G.R., 1982. Platelet-derived growth factor in chemotaxis for fibroblasts. *J. Cell Biol.* 92, 584–588.
- Tranquillo, R.T., Murray, J.D., 1992. Continuum model of fibroblast-driven wound contraction: inflammation-contraction. *J. Theoret. Biol.* 158 (2), 135–172.
- Valero, C., Javierre, E., García-Aznar, J.M., Gomez-Benito, M.J., 2014. A cell regulatory mechanism involving feedback between contraction and tissue formation guides wound healing progression. *PLOS ONE* 9 (3), e92774.
- Valero, C., Javierre, E., García-Aznar, J.M., Gomez-Benito, M.J., Menzel, A., 2015. Modeling of anisotropic wound healing. *J. Mech. Phys. Solids* 79, 80–91.
- Vermolen, F.J., Gefen, A., 2012. A semi-stochastic cell-based formalism to model the dynamics of migration of cells in colonies. *Biomech. Model. Mechanobiol.* 11 (1–2), 183–195.
- Vermolen, F.J., Gefen, A., 2015. Semi-stochastic cell-level computational modelling of cellular forces: application to contractures in burns and cyclic loading. *Biomech. Model. Mechanobiol.* 14 (6), 1181–1195.